A new methodology for the reduction of vibrational kinetics in non-equilibrium microwave plasma

Application to CO_2 dissociation

Fernández de la Fuente, Javier; Moreno Wandurraga, Sergio; Stankiewicz, Andrzej; Stefanidis, Georgios

DOI
10.1039/C6RE00044D

Publication date
2016

Document Version
Accepted author manuscript

Published in
Reaction Chemistry & Engineering

A new methodology for the reduction of vibrational kinetics in non-equilibrium microwave plasma: Application to CO_2 dissociation.

J F de la Fuente[1,#], S H Moreno [1,#] and G D Stefanidis[1,2,*]

[1] *Intensified Reaction & Separation Systems, Process & Energy Laboratory, Delft University of Technology, Leeghwaterstraat 39, 2628 CB, Delft, The Netherlands*

[2] *Chemical Engineering Department, Katholieke Universiteit Leuven, Celestijnenlaan 200f, 3001 Leuven (Heverlee), Belgium*

* Corresponding author: Georgios D. Stefanidis, e-mail: georgios.stefanidis@cit.kuleuven.be

# The first two authors had equal contribution to the work

Abstract

Plasma reactor technologies have the potential to enable storage of green renewable electricity into fuels and chemicals. One of the major challenges for the implementation of these technologies is the energy efficiency. Empirical enhancement of plasma reactors performance has proven to be insufficient in this regard. Numerical models are becoming therefore essential to get insight into the process for optimization purposes. The chemistry in non-thermal plasmas is the most challenging and complex part of the model due to the large number of species and reactions involved. The most recent reaction kinetic model for carbon dioxide (CO_2) dissociation in non-thermal microwave plasma considers more than one hundred species and thousands of reactions. To enable the implementation of this model into multidimensional simulations, a new reduction methodology to simplify the state-to-state kinetic model is presented. It is based on four key elements; 1) all the asymmetric vibrational levels are lumped within a single group, or fictitious species, CO_2*, 2) this group follows a non-equilibrium Treanor distribution, 3) an algebraic approximation is used to compute the vibrational temperature from the translational temperature based on the Landau-Teller formula and 4) weighted algebraic expressions are applied, instead of complex differential equations, to calculate the rates of the most influencing reactions; this decreases substantially the calculation time. Using this new approach, the dissociation and vibrational kinetics are captured in a reduced set of 44 reactions among 13 species. The predictions of the reduced kinetic model regarding the concentrations of the heavy species in the afterglow zone are in good agreement with those of the detailed model from which the former was derived. The methodology may also be applied to other state-to-state kinetic models in which interactions of vibrational levels have the largest share in the global set of reactions.

Keywords

CO_2 utilization, non-equilibrium microwave plasma, plasma kinetics, kinetic model reduction

Introduction

Two major environmental and scientific challenges faced nowadays are energy storage and greenhouse gas emissions [1-5]. The pressing need in employing renewable energy sources has brought up new challenges regarding electricity storage, which need to be overcome before the current energy mix can be upgraded to one based on renewable energy sources [3]. Various alternatives are being investigated such as mechanical, chemical, electromagnetic and thermal storage [3-6]. The valorisation of carbon dioxide (CO_2) to produce synthetic fuels has been identified as one of the approaches to convert renewable electricity surplus into easy-to-store chemicals [6]. In this regard, plasma-based systems combine the opportunity of utilizing both electricity surplus as well as greenhouse gases, as feedstock, for the conversion process. Plasma reactor technology offers potential benefits, such as compactness, robustness and fast response time to temporal variations at the reactor inlet [7, 8]. Therefore, it is a suitable technology to cope with the intermittent and fluctuating pattern of renewable energy supply (e.g., solar and wind energy) [2, 9]. Moreover, the characteristics of non-thermal plasma are particularly favourable for the dissociation and utilization of CO_2, making it a very promising technology for chemical process intensification.

One of the major drawbacks to commercialize plasma technology is the high energy consumption [10]. Despite the extensive research conducted experimentally to optimize plasma reactor performance [11, 12], there are still a lot of uncertainties that need to be addressed in order to fully understand the reaction mechanisms in non-thermal plasma conditions and optimize plasma processes [13]. Therefore, there is a need to develop reliable plasma chemistries that can be implemented in plasma reactor models for evaluation of different reactor configurations and process optimization [1]. Predictive plasma reactor models are inherently multiphysics models describing electromagnetic wave propagation, mass conservation, electron and fluid dynamics, heat transfer and plasma chemical kinetics [14-16]. When detailed kinetic models, including all the elementary steps, are taken into account, the model becomes highly complex due to the large number of reactions and species needed to describe the plasma reactive system. Large chemical kinetic models require solution of a large number of transport equations in addition to estimating the chemical source terms, often governed by stiff ordinary differential equations (ODEs) [17]. Hence, to enable the applicability of plasma kinetic models in multidimensional simulations, a simplification approach to reduce complex kinetic models is presented in this work.

Several attempts have been made to develop reaction kinetic models for CO_2 chemistry. In [18], a numerical model for the plasma-chemical reactions taking place in a pure CO_2 glow discharge was developed, albeit vibrational kinetics were not included. In [19], a high temperature non-equilibrium reacting CO_2 flow was studied; although a detailed description of the vibrational kinetics by means of kinetic theory methods was given, the plasma chemistry was missing. More recently, a state-to-state

kinetic model including all the relevant chemical reactions in a CO_2 non-thermal microwave discharge was proposed [20]. In a subsequent publication [21], the kinetic model was updated to evaluate the energy efficiency in the discharge. This model consists of 126 species and more than 10000 reactions, including electron impact, neutrals and vibrational energy transfer reactions. In [9], a reduced kinetic model for CO_2 dissociation in dielectric barrier discharges (DBD) was introduced. This model includes the most relevant plasma species and reactions in DBD discharge conditions, but lacks vibrational kinetics. Such a model is then unsuitable for microwave discharges where dissociation through vibrational excitation of the molecule appears to be the most efficient dissociation mechanism [11, 22].

Up to date, a practical and manageable kinetic model for CO_2 dissociation in non-thermal microwave plasma has not been reported. In this work, a novel two-step approach for reduction of vibrational kinetics is presented and applied to CO_2 dissociation in non-equilibrium microwave discharges. Two different simplification techniques are coupled to carry out the reduction process: i) chemical lumping of species, where several species are grouped into a single pseudo-species, in combination with ii) a skeletal reduction approach, which includes identification and selection of the most influencing species in the dissociation process without loss of qualitative potential [1, 19, 23]. The novelty of the presented model lies in four key elements; 1) all the asymmetric vibrational levels are lumped within a single group instead of several groups as reported in [24-26], 2) this group follows the non-equilibrium Treanor distribution, 3) an algebraic approximation is used to compute the vibrational temperature from the translational temperature based on the Landau-Teller formula and 4) weighted algebraic expressions are applied, instead of complex differential equations, to calculate the rates of the most influencing reactions. The obtained kinetic model comprises 13 species and 44 reactions whereby all the relevant chemical reactions influencing the CO_2 dissociation process are accounted for. The comparison of the results given by the detailed and reduced kinetic models shows good agreement. In particular, the best match is obtained in the afterglow zone, where the species concentrations represent those at the outlet of the reactor. It is important to remark that the purpose of the work is to explore and validate a new methodology for the reduction of vibrational plasma kinetics, exemplified herein for a CO_2 non-thermal microwave discharge, rather than performing self-consistent multidimensional simulations, a task that has not been carried out yet.

Description of the model

To properly evaluate non-equilibrium reaction kinetics, state-to-state (STS) kinetic models are developed accounting for all the internal excited states and their interactions. This approach leads to reaction mechanisms with a large number of species (in the order of dozens to hundreds) and reactions

(in the range of hundreds to thousands), which are not practical for multidimensional simulations. Therefore, the application of STS kinetic models have been mostly limited to zero and one-dimensional simulations. The STS kinetic model reported in [21] was taken as starting point in this work. In the following subsection, a detailed description of the plasma chemical reactive system and also the simplification methodoly is given.

Reduced plasma kinetic model: species and reactions

The species considered in the reduced kinetic model are displayed in Table 1. As stated in [12, 27], the CO_2 molecule presents three normal vibrational modes, the symmetric bending mode, the symmetric stretch mode and the asymmetric stretch mode. The symmetric modes of vibration of this molecule are herein denoted as CO_2v_a, CO_2v_b and CO_2v_c (Table 1). The asymmetric stretch mode is found to be the most energy efficient dissociation channel due to its capacity to store vibrational energy. In this mode, 21 vibrational excited levels are considered up to the dissociation limit of the molecule [20]. The reduction potential of the model is based on the lumping of all the asymmetric vibrational excited levels into a fictitious species, referred to as CO_2*. This leads to a substantial simplification of the STS kinetic model, as most of the reactions come from the state-to-state interactions of vibrational levels [28].

Table 1. Chemical species included in the reduced kinetic model. CO_2v_a, CO_2v_b and CO_2v_c are the symmetric modes of vibration whereas CO_2* represents a fictitious species accounting for all the asymmetric vibrational levels.

Type	Species
Neutral ground states	CO_2, CO, O, O_2
Vibrationally excited states	CO_2v_a, CO_2v_b, CO_2v_c, CO_2*
Charged species	CO_2^+,CO^+,O_2^+,O^+,e

The reactions included in the reduced kinetic model are shown in Tables 2, 3, 4 and 5. In this model, four different types of reactions are included; these are electron impact reactions, reactions of neutral species, vibrational energy exchange reactions and surface reactions, which are presented in Tables 2, 3, 4 and 5, respectively.

Electron impact reactions form the driving force of the plasma. The electrons gain kinetic energy from the electromagnetic field, which is further transferred to other species through collisions. The generation of new electrons occurs via ionization reactions, which are responsible for sustaining the plasma.

Table 2. Electron impact reactions (RX) considered in the reduced kinetic model.

N°	Process	Reaction	Cross section
RX1	CO_2 Elastic scattering	$e + CO_2 \rightarrow e + CO_2$	[29]
RX2	CO_2* Elastic scattering	$e + CO_2^* \rightarrow e + CO_2^*$	Same as RX1
RX3	CO Elastic scattering	$e + CO \rightarrow e + CO$	[30, 31]
RX4	O Elastic scattering	$e + O \rightarrow e + O$	[31]
RX5	O_2 Elastic scattering	$e + O_2 \rightarrow e + O_2$	[32]
RX6	CO_2 Ionization	$e + CO_2 \rightarrow e + e + CO_2^+$	[29]
RX7	CO_2 Ionization from CO_2*	$e + CO_2^* \rightarrow e + e + CO_2^+$	Same as RX6
RX8	CO Ionization	$e + CO \rightarrow e + e + CO^+$	[30]
RX9	O Ionization	$e + O \rightarrow e + e + O^+$	[33]
RX10	O_2 Ionization	$e + O_2 \rightarrow e + e + O_2^+$	[32]
RX11	Vibrational (de) excitation to CO_2v_a	$e + CO_2 \leftrightarrow e + CO_2v_a$	[29]
RX12	Vibrational (de) excitation to CO_2v_b	$e + CO_2 \leftrightarrow e + CO_2\ v_b$	[29]
RX13	Vibrational (de) excitation to CO_2*	$e + CO_2 \leftrightarrow e + CO_2^*$	Section "Simplification approach"

Reactions of neutral species play an important role in the formation of reactive species to promote chemical reactions. At favourable dissociation conditions, a fraction of the energy transferred from the electrons to the CO_2 molecule is stored as internal energy in high vibrational levels of the asymmetric mode, which can either facilitate its dissociation or be transferred to the bulk gas as heat.

Table 3. Reactions of neutrals (RN) included in the model. M = CO_2, CO or O_2. Gas temperature (T_g) in K and rate constants in cm^3/s and cm^6/s for binary and ternary reactions, respectively.

N°	Process/Reaction	Rate constant
RN1	CO_2* Dissociation by collisions with CO_2, CO and O_2 $CO_2^* + M \rightarrow CO + O + M$	$9.59 \times 10^{-16} (T_g/300)^{2.92} \exp(639/T_g)$
RN2	CO_2* Dissociation by collisions with O $CO_2^* + O \rightarrow CO + O_2$	$3.35 \times 10^{-14} (T_g/300)^{1.47} \exp(-271/T_g)$
RN3	Three-body CO and O recombination $CO + O + M \rightarrow CO_2 + M$	$8.2 \times 10^{-34} \exp(-1510/T_g)$
RN4	Two-body CO and O_2 recombination $CO + O_2 \rightarrow CO_2 + O$	$1.23 \times 10^{-12} \exp(-12800/T_g)$
RN5	Three-body O recombination $O + O + M \rightarrow O_2 + M$	$1.27 \times 10^{-32} (T_g/300)^{-1} \exp(-170/T_g)$

Vibrational energy transfer reactions are responsible for the energy exchange between vibrationally excited molecules and the vibrational energy loss to ground state molecules. In this model, these

reactions mainly lead to generation of heat by transferring the energy to the bulk gas via vibrational-translational (VT) relaxation reactions. Note that the parameters v_{s2} and v_{s3} represent the stoichiometric coefficients of the symmetric excited states for reactions RV2 and RV3, whereas v_{l2} and v_{l3} indicate the stoichiometric coefficients of the lumped excited state for the same reactions (RV2 and RV3).

Table 4. Vibrational energy transfer reactions (RV) considered in the model. M = CO_2, CO or O_2. Gas temperature (T_g) in K. v_{s2}, v_{s3}, v_{l2} and v_{l3} represent the stoichiometric coefficients of the symmetric excited states (s) and the lumped excited state (l), respectively, for the reactions RV2 and RV3.

N°	Process/Reaction	Rate constant
RV1	VT Relaxation of symmetric vibrationally excited states x = a,b,c	
	$CO_2v_x + M \rightarrow CO_2 + M$	$7.14 \times 10^{-8} \exp(-177T_g^{-1/3} + 451T_g^{-2/3})$
	$M = CO_2$	x 1
	$M = CO, O_2$	x 0.7
RV2	VT Relaxation of the lumped asymmetric vibrationally excited state	
	$CO_2^* + M \rightarrow v_{l2}\, CO_2^* + v_{s2}\, (CO_2v_a + CO_2v_b + CO_2v_c) + M$	
	$M = CO_2$	$4.72 \times 10^{-17} (T_g/300)^{6.55} \exp(1289/T_g)$
	$M = CO$	$1.47 \times 10^{-17} (T_g/300)^{6.53} \exp(1282/T_g)$
	$M = O_2$	$1.95 \times 10^{-17} (T_g/300)^{6.53} \exp(1282/T_g)$
RV3	VV' Relaxation between symmetric and asymmetric vibrationally excited states	$3.99 \times 10^{-15} (T_g/300)^{4.46} \exp(398/T_g)$
	$CO_2^* + CO_2 \rightarrow v_{l3}\, CO_2^* + v_{s3}\, (CO_2v_a + CO_2v_b)$	

The charged species, electrons and ions, diffuse together toward the walls by the effect of ambipolar diffusion, where electrons and ions are recombined via collisions on the reactor wall.

Table 5. Surface reactions (RS) included in the reduced kinetic model

N°	Process	Reaction	Sticking coefficient (γ)
RS1	CO_2^+ Neutralization	$CO_2^+ \rightarrow CO_2$	1
RS2	CO^+ Neutralization	$CO^+ \rightarrow CO$	1
RS3	O^+ Neutralization	$O^+ \rightarrow O$	1
RS4	O_2^+ Neutralization	$O_2^+ \rightarrow O_2$	1

Using the simplification approach, which is described in the following sections, the STS model has been significantly reduced to 44 reactions among 13 species accounting for the most relevant processes that dominate the dissociation of CO_2 in non-equilibrium microwave plasma. A schematic representation of the reaction pathway is presented in Fig. 1.

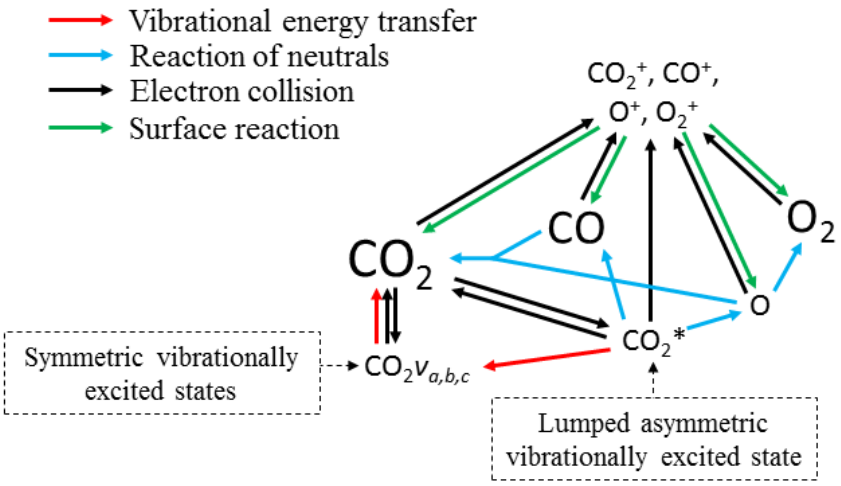

Fig. 1. Reaction pathway of the reduced kinetic model.

Simplification approach

Up to date, various approaches have been adopted to reduce STS kinetic models. For instance, in [28], the Principal Component Analysis (PCA) is applied to the CO_2 dissociation process driven by vibrational kinetics; in this approach, a large database of results obtained with the STS kinetic model is required to identify the principal components. One can also make use of commercially available software, such as CHEMKIN-PRO [34], which is mainly used for combustion processes, and PumpKin [35], which employs algorithms to identify key components and group large set of reactions in reduced reaction pathways; the latter is mostly used in plasma chemical models. The approaches in [36] and [37] are closer to the one presented here; specifically, the kinetics are described by the vibrational and translational temperatures for the dissociation and recombination regimes of N_2 + N in non-equilibrium hypersonic flows. Approaches where internal modes of molecules are divided into several groups have been reported as well [24-26]. Such a multigroup lumping method was recently applied to reduce the vibrational kinetics of CO_2 [38]. In this method, the vibrational levels of the asymmetric mode are lumped into various groups, each characterized by an internal Boltzmann equilibrium distribution given by its own vibrational temperature.

In this work, a new reduction approach is introduced to simplify the STS kinetic model proposed in [21] for the dissociation of CO_2 in non-equilibrium microwave discharges. As opposed to [24-26], our approach is based on lumping all the asymmetric vibrational levels within a single group. In addition, a non-equilibrium distribution, the so-called Treanor distribution, is considered in the lumping process instead of the commonly used Boltzmann distribution. It is known that the Treanor distribution overestimates the population of high energy levels, yet, this is balanced by the high VT and VV' rates obtained for the group (see section Simplification approach). The complexity of multi-temperature approaches, widely used up to now, is reduced by the introduction of an algebraic approximation

linking the vibrational and translational temperatures. Another advantange of this methodology is the implementation of weighted algebraic expressions to compute rate constants, instead of solving the complex differential equations used in [24-26], thereby enabling a faster calculation of the reaction rates. The application of this technique results in significant simplification regarding the number of reactions and species to describe the dissociation of CO_2. Few methods have succeeded in the reduction of detailed plasma kinetic models, which concern mainly diatomic molecules. In the case of more complex molecules, the development of practical and manageable approaches is subject to ongoing research in order to enable multidimensional modeling of non-equilibrium plasma processes.

As stated before, the main reduction in the presented approach is achieved by grouping the asymmetric vibrationally excited states of CO_2, which represent the main dissociation channel of the molecule in this type of discharges. Hence, the 21 vibrational levels considered in the detailed kinetic model [21] to describe the dissociation processes are lumped into a single asymmetric vibrational excited state. The fictitious species (CO_2*) is the representation of all asymmetric vibrational excited states that are not in thermal equilibrium with the translational energy mode of the molecule. An illustration of the lumped species is outlined in Fig. 2.

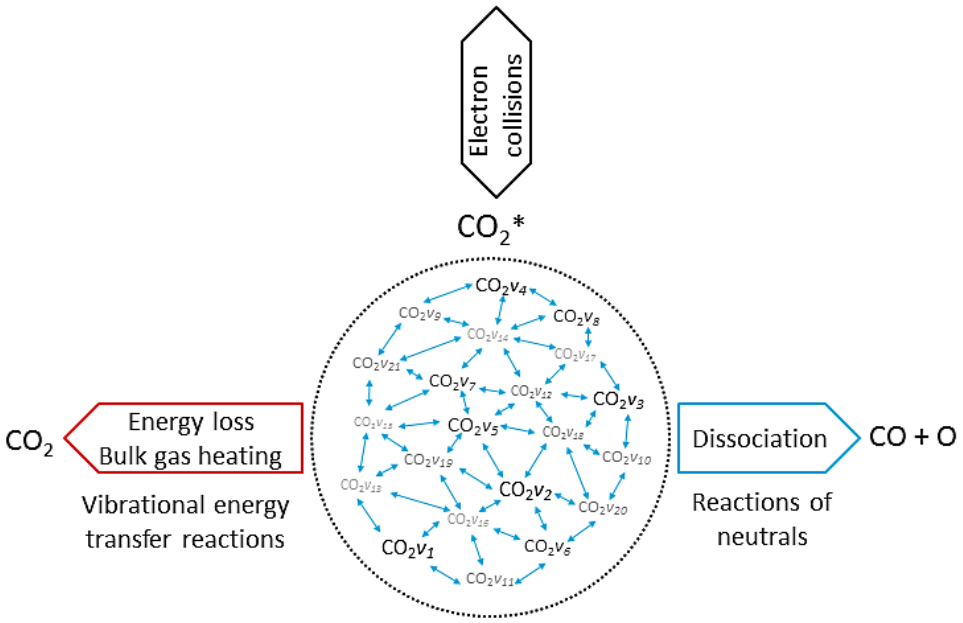

Fig. 2. Lumping of 21 asymmetric vibrational levels into a fictitious species CO_2*.

High CO_2 dissociation rates can be attained when the high vibrational levels of CO_2 remain far from equilibrium [21]. In low temperature plasmas, the highest relaxation rate is the (vibrational-vibrational) VV relaxation, i.e. the interaction of CO_2 molecules that are excited in the same vibrational mode. When the temperature of the gas increases, the (vibrational-translational) VT relaxation rate is boosted, thus leading to a high energy loss by heating up the gas. It is assumed that the vibrational levels lumped into the fictitious species CO_2* solely exchange energy through VV relaxation.

Although, as a group, they can either dissociate or lose energy via VT relaxation as shown in Fig. 2. One of the major assumptions taken in the presented model is that the excited states follow the so-called Treanor non-equilibrium distribution [39], which allows for the calculation of the population densities of all asymmetric vibrationally excited states. The reason behind this assumption is the dominant vibrational energy transfer mechanism in the discharge: electron impact vibrational excitation (0→1) followed by VV relaxation. Hence, the energy used in the dissociation is mainly transferred through this mechanism, which also results in a Treanor vibrational distribution. For simplicity, a good approximation is to fit their energy levels to a diatomic anharmonic oscillator model and compute an effective anharmonicity coefficient so that the Treanor distribution can be calculated. The Treanor distribution enables the evaluation of the departure from thermal equilibrium given by the Boltzmann distribution. Fig. 3 shows this concept more in detail by plotting the vibrational distribution functions considering different approaches: 1) Boltzmann distribution, 2) STS kinetic model [20] (microwave discharge, power density = 25 W cm^{-3} and 0.8 ms time) and 3) Treanor distirbution. The T_v/T_g value shown in Fig. 3 do not correspond to the values used to carry out the validation of the model, instead it shows the qualitative difference of the various VDF's. At low T_v/T_g values, the Treanor distribution approaches the Boltzmann distribution (becoming equal when $T_v/T_g = 1$), whereas at high T_v/T_g values the highly non-equilibrium nature of the discharge is noticeable. The departure from thermal equilibrium observed for both the STS and Treanor vibrational distributions represents the stored vibrational energy in the asymmetric mode. In comparison to the Treanor distribution the high levels of the STS distribution are depleted due to VT relaxation and dissociation. Herein, the overpopulation of the Treanor distribution is used to compute effective rates for vibrational relaxation and dissociation.

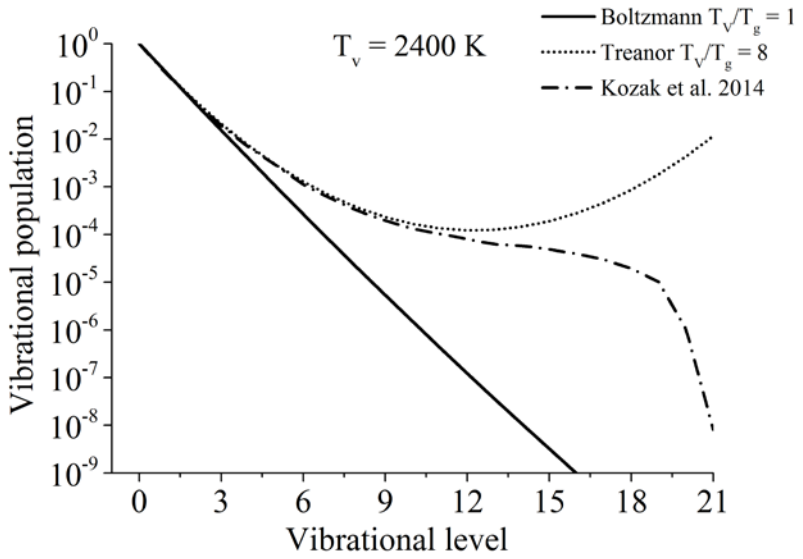

Fig. 3. Comparison of the vibrational distributions functions considering the approaches: 1) Boltzmann distribution, 2) STS kinetic model [20] (microwave discharge, power density = 25 W cm^{-3}) and 0.8 ms time) and 3) Treanor distribution.

The vibrational and bulk gas temperatures (T_v and T_g) are required to calculate the Treanor distribution, which reads [39]:

$$n_v = n_0 \exp\left(-\frac{vE_1}{T_v} + \frac{vE_1 - E_v}{T_g}\right) \quad (1)$$

where n_v is the population density and E_v the energy in eV of the vibrational level v, n_0 is the population density of the CO_2 ground state and T_g and T_v are the bulk gas and the vibrational temperatures (both in eV), respectively. The vibrational temperature in the previous equation is based on the population density of the first vibrational level and it is computed as follows

$$T_v = \frac{E_1}{\ln\left(\frac{n_0}{n_1}\right)} \quad (2)$$

The discharge can be characterized by the T_v/T_g ratio, which should be high enough at low bulk gas temperatures to achieve efficient dissociation. For multidimentional models this mean or characteristic value of the discharge could be used for the calculations, instead of considering spatial variations of the T_v/T_g values throughout the discharge. Considering the conditions studied in [21], T_v/T_g values lie in the range of 5.2 to 7. A sensitivity analysis carried out to study the effect of this value on the kinetics yielded the best agreement with a value of 6 (see Validation of the model section). On the other hand, at temperatures beyond the characteristic vibrational temperature, the VT and VV relaxation processes become comparable, even for the lowest vibrational levels [39]. In this case, the non-thermal effect is not attained and the discharge is completely thermalized, T_v/T_g=1. The conditions at which a plasma reaches thermal equilibrium vary depending on the type and duration of the discharge. Since it is rather complex to determine when a microwave plasma reaches thermal equilibrium (between 4000 to 5000 K [12]), a value of 5070 K is assumed. This temperature is 1.5 times the characteristic vibrational temperature of CO_2 and is above 5000 K, which ensures thermal equilibrium conditions of the plasma (dominance of VT over VV relaxation). Moreover, as found in [40], the gas temperature in a pure CO_2 microwave plasma torch is about 5000 K, which is consistent with our assumption. For further clarification, a comparison of the influence of these two parameters is given in the subsequent section, in which it is shown that the gas temperature at which quasi-equilibrium plasma conditions are reached barely has any influence on the results, while the high T_v/T_g value affects the calculations to a higher degree. The accuracy of the values chosen to compute the Treanor distribution is of secondary importance for the scope of this work, which is to demonstrate the validity of the reduction methodology.

Another point of discussion is the shape of the curve to estimate the T_v/T_g ratio. An exponential dependence is proposed as an initial approximation based on the Landau-Teller temperature dependence of vibrational-translational relaxation (VT), which becomes more relevant as temperature increases. Besides, a simple expression is preferred so that only two points are required for the fitting (see Fig. 4). For the considered range of temperatures the following expression gives a reasonable agreement of the temperature dependence with STS calculations of CO_2 vibrational kinetics

$$T_v/T_g = a \exp\left(\frac{b}{T_g{}^{1/3}}\right) \times \frac{1}{T_g} = 10937 \exp\left(\frac{-12.05}{T_g{}^{1/3}}\right) \times \frac{1}{T_g} \quad (3)$$

An accurate description of T_v and T_g would require the full set of reactions, which is not practical, or even possible, for multidimensional simulations. The coefficients *a* and *b* were computed by fitting this function to the proposed values of T_v/T_g. By following this approach, the Treanor distribution becomes exclusively a function of the gas temperature, thereby facilitating the calculation of the distribution. The Treanor distribution at various gas temperatures enables the estimation of rate constants for reactions involving the fictitious species CO_2*. These parameters are obtained by adding the individual contributions of the vibrational levels, which are computed from their populations and individual rate constants.

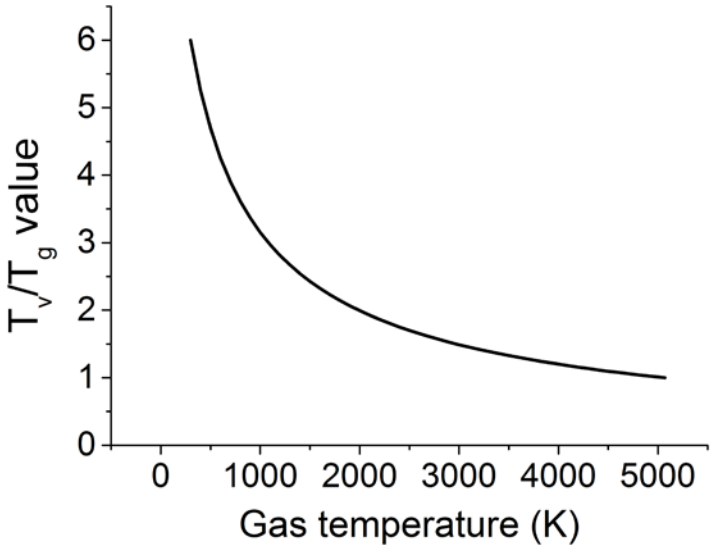

Fig. 4. T_v/T_g ratio-gas temperature dependence according to equation (3).

Electron impact reactions

One of the major simplifications in the reduced kinetic model is accomplished by assuming a Maxwellian electron energy distribution function (EEDF) This approximation is commonly accepted for typical microwave discharges as shown in [41], where a comparison between Maxwellian and non-equilibrium EEDFs is carried out. The studied microwave discharges present typical electron

temperature values in the range 0.5 to 2 eV, in which the Maxwellian EEDF is rather similar to the non-equilibrium EEDF. Nevertheless, careful consideration should be given to this assumption, as reported in [42], where it was shown that non-equilibrium distributions can present an overpopulation in the tail, i.e. at high electron energies, as compared to a Maxwellian EEDF. These overpopulated tails are caused by superelastic collisions with electronically excited states and can influence high-threshold electron impact processes, resulting in increase in their reaction rates.

At low electron energies, the highest reaction rates are expected for elastic scattering and vibrational excitation since these reactions show the largest collisional cross sections [43]. On the other hand, at high electron energies, the EEDF is considerably smaller, meaning that the rate constants are orders of magnitude smaller than processes taking place at low energies. For instance, for an electron temperature of 2 eV, the rate coefficient of the electron impact CO_2 dissociation, which takes place at relatively high electron energies, is 3 orders of magnitude smaller than the rate coefficient of vibrational excitation. Therefore, only reactions with large cross sections are considered in the high electron energy range. In particular, besides elastic scattering, the largest cross section and the lowest energy threshold is attributed to the single charge ionization of CO_2 [29]. In fact, the ionization rate due to single charge ionization is at least two orders of magnitude larger than other ionization processes, such as dissociative ionization or multiple charge ionization. In conclusion, three types of collision processes (elastic scattering, vibrational excitation and non-dissociative single charge ionization) are taken into account for the reduced kinetic model.

Concerning collisions of electrons with the main neutral products of CO_2, i.e. CO, O, O_2 and O_3, these species take part in important processes of the reactive system, thus displaying high population densities. Based on the results given in [21], the population density of O_3 is at least two orders of magnitude less than that of O_2 and three orders of magnitude less than the one of CO_2. Moreover, O_3 is mainly a product formed in the afterglow and does not have a major influence on the dissociation kinetics of CO_2. For this reason, the O_3 species is not included in the model. By analysing the cross section data reported [30-33, 43, 44], it can be concluded that the same type of reactions (elastic scattering, vibrational excitation and ionization) should be considered for the neutral species.

It is noted that the electronic excitation process has been neglected for neutral species in the reduced kinetic model, as it barely influences the CO_2 dissociation kinetics at low electron energies. Furthermore, assuming quasi-neutrality of plasma and an ionization degree of about 10^{-5}, [21] the mass fractions of the charged species are ~5 orders of magnitude lower than the neutrals. Therefore, reactions with charged species are not included in the model.

With regard to electron collisions with vibrationally excited species, vibrational excitation reactions are considered for CO_2 and neglected for other neutrals as the energy transfer to vibrational modes of

these species is considerably lower [21]. While the symmetric vibrational modes of CO_2, CO_2v_a and CO_2v_b, in combination with the lumped asymmetric vibrational mode CO_2*, are included, higher symmetric levels, such as the CO_2v_c and CO_2v_d are not added, as the cross sections for multiquantum vibrational jumps are smaller than single quantum vibrational jumps. Reverse processes of vibrational excitation, called de-excitation reactions, are also included in the model by using the detailed balancing principle [45].

The black arrows in Fig. 1 show the electron impact reactions included in the reduced kinetic model. A total of 16 electron impact reactions are included; we refer to Table 2 for more information.

*Cross section calculation for vibrational excitation from CO_2 to CO_2**

An overall vibrational excitation cross section is computed by lumping the vibrational excitation processes in the asymmetric vibrational mode, from the CO_2 ground state to the higher states within CO_2*. Vibrational de-excitation cross sections are obtained from the overall cross section by applying the detailed balancing principle. The calculation is carried out by scaling the cross sections using the Fridman's approximation. Then, the computed cross sections are added to estimate the overall cross section. The total electron impact vibrational excitation rate for CO_2 is the sum of the vibrational excitation rates from level 0 to all higher levels, thus:

$$n_0 n_e \sum_{j=1}^{21} k_{0,j} = n_0 n_e \gamma \int_0^{\infty} \varepsilon \sigma_V(\varepsilon) f(\varepsilon) d\varepsilon \tag{4}$$

where n_0 is the population density of the vibrational level 0 (CO_2); n_e is the population density of electrons; $k_{0,j}$ is the rate coefficient for the vibrational excitation from level 0 to level j; ε is the electron energy; $\sigma_{0,j}(\varepsilon)$ is the cross section for the vibrational excitation from level 0 to level j; f(ε) is the electron energy distribution; γ is a conversion units constant and $\sigma_V(\varepsilon)$ is the cross section for the excitation of CO_2 to CO_2* (reaction RX13 in Table 2) and is computed as follows:

$$\sigma_V(\varepsilon) = \sum_{j=1}^{21} \sigma_{0,j}(\varepsilon) \tag{5}$$

Not all the cross sections for the transitions from any level i to a higher level j are available. Hence, they are computed using the Fridman's approximation [12]. Specifically, the cross section of the lowest transition, from level 0 to level 1 ($\sigma_{0,1}$), is scaled to higher transitions by applying the following expression:

$$\sigma_{i,j}(\varepsilon + E_{i,j} - E_{0,1}) = \sigma_{0,1}(\varepsilon)\, exp\left(\frac{-\alpha(j-i-1)}{1+\beta i}\right) \tag{6}$$

where $E_{i,j} = E_j - E_i$ is the energy difference between levels j and i and α and β are scaling factors. For the specific case of CO_2, the α factor takes the value of 0.5 and the β factor is assumed to be 0 [12, 20]. This approximation is used to compute all the transitions from level 0, which are subsequently added to obtain σ_v. The cross section's magnitude increases as a consequence of adding the cross sections of multiquantum vibrational jumps, while the discrete energy levels explain the presence of multiple peaks. The values of $\sigma_{0,1}$ used in the calculations are taken from [29].

In Fig. 5, a comparison between the cross section for the transition from level 0 to level 1 and the cross section for the excitation from CO_2 to CO_2* is presented. The energy threshold of the process is the minimum energy required to put a CO_2 molecule into vibration, which in this case is $E_1 - E_0 = 0.29$ eV.

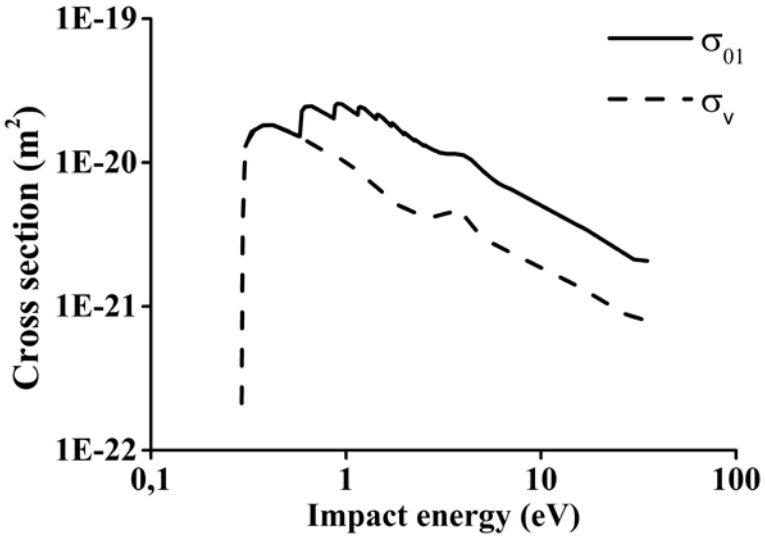

Fig. 5. Cross section for the vibrational excitation from CO_2 to CO_2*.

Reactions of neutral species

As mentioned in the previous section, a large portion of the energy is transferred from the electrons to the vibrational modes of the CO_2 molecule. Once the asymmetric mode is energized, the stored vibrational energy can be utilized to dissociate the molecule. A total of 11 dissociation and recombination reactions with neutrals are included in the reduced kinetic model (see blue arrows in Fig. 1 and Table 3). When compared to the STS kinetic model, three neutrals species (C, C_2O and O_3) are disregarded. The reason to neglect these species is the low net production rates and therefore the very low population densities (5 orders of magnitude smaller than CO_2) displayed in the overall reaction scheme. Moreover, these species show a minor influence on the dissociation kinetics. The reactions of neutral species are then restricted to the ones involving CO_2, CO, O and O_2.

In Fig. 1, it can be observed that the lumped excited species CO_2* is considered in the dissociation processes as dissociation reactions involving CO_2 ground state (v = 0) present the highest activation energies leading to very low reaction rates.

Due to the change in the activation energy of the dissociation reactions, as a consequence of the stored vibrational energy, the rate constants of reactions RN1 and RN2 must be computed. To estimate the efficiency in the reduction of the activation energy due to vibrational excitation, the Fridman-Macheret α-model is applied [12]. The following expression is used [46]:

$$k_v(E_v, T_g) = A \exp\left(-\frac{E_a - \alpha E_V}{T_g}\right) \tag{7}$$

where A is the conventional pre-exponential factor, E_a is the activation energy of the reaction in K, E_v is the vibrational energy of level v in K (energy levels given in [20]), T_g is the bulk gas temperature in K and α is the efficiency of the vibrational energy in reducing the activation energy. The α values for RN1 (α = 1) and RN2 (α = 0.5) are taken from [20].

The rate constants of each level are then multiplied by the population densities obtained from the Treanor distribution. For the dissociation reaction RN1, the following equation is apllied [37]:

$$k(T_g) = \sum_{v=1}^{21} n_v(T_g) k_v(E_v, T_g) \tag{8}$$

For the dissociation reaction RN2, a different expression is used. RN1 is an endothermic reaction with a high activation energy, which virtually vanishes at the highest vibrational levels, whereas RN2 is a thermoneutral reaction with an activation energy that vanishes at vibrational levels above v = 10. Hence, the form of the rate constant is divided into two groups: 1) vibrational levels from 0 to 10 and 2) levels from 11 to 21.We propose the following expression to compute the rate constant for RN2:

$$\ln k(T_g) = \frac{v_1}{v_2} \ln k_1(T_g) + \frac{v_2 - v_1}{v_2} \ln k_2 \tag{9}$$

where v_1 is the number of levels in the first group and v_2 the number of levels in the second group; k_1 is the averaged rate constant of the first group and k_2 the one of the second group. Lastly, the averaged rate constant is estimated by adding the individual contributions of the lumped vibrational levels (v = 1 – 21). This process is repeated at various temperatures within the range of interest, 300 – 1500 K. Note that the validity of the rate constant expressions considered for the vibrational energy exchange reactions lies in the range 300 to 1500 K [47], which hinders the evaluation of this model at higher gas temperatures.

In Fig. 6, the calculated rate constants for the reactions RN1 and RN2 at different temperatures are displayed. These values are then fitted to a modified Arrhenius type of equation so that a single temperature-dependent expression for the CO_2* dissociation reactions can be implemented (Table 3, RN1 and RN2 rate constants).

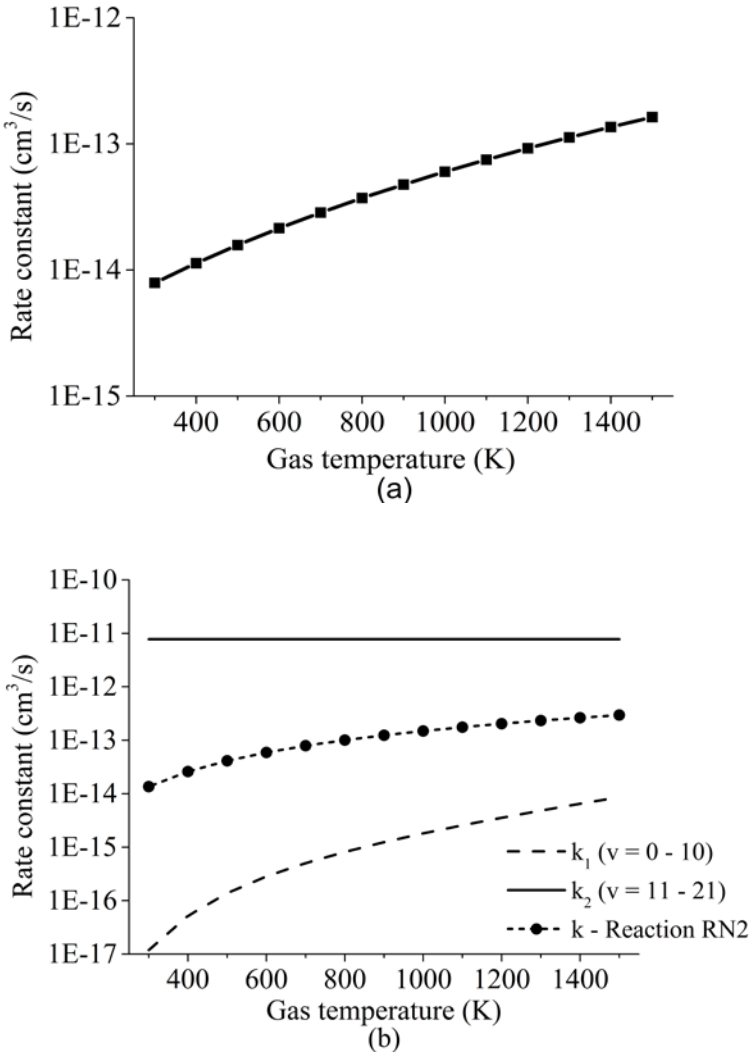

Fig. 6. (a) Rate constant of reaction RN1 as function of gas temperature and **(b)** rate constant of reaction RN2 as function of gas temperature (k_1 and k_2 are shown for reference).

Vibrational energy transfer reactions

The outcome of these energy exchange processes is mainly related to energy loss from vibrationally excited states to the bulk gas. Two types of relaxation reactions are considered, VT and VV' relaxation. In the VT type, vibrational and translational degrees of freedom exchange energy in which either a symmetric vibrationally excited state loses its energy in a collision with a neutral ground state (RV1) or the lumped asymmetric excited state transfers a fraction of its vibrational energy to the symmetric vibrational modes $CO_2v_{a,b,c.}$(RV2). The VV' relaxation process (RV3) comprises the energy

exchange due to collisions between the lumped excited state CO_2* and a CO_2 ground state, thus transferring a portion of its vibrational energy to the symmetric modes of the molecule. A total of 13 vibrational energy exchange reactions are included in the reduced kinetic model (red arrows in Fig. 1 and Table 4). The following subsections describe how the rate constants for the reactions RV2 and RV3 are calculated. The energy change in the reactions is fitted to diatomic anharmonic oscillator models so that the anharmonicity coefficient can be computed to scale the rate constants from the lowest vibrational state to higher ones at specific gas temperatures [20]. The approach to calculate these rates is rather similar to the one used for the reaction of neutrals with one difference; the stoichiometric coefficients also depend on the Treanor distribution, which then depends on the bulk gas temperature.

Rate constant for reaction RV2

The initial step is to compute the rate constants of the VT relaxation reactions for all the asymmetric vibrational levels within CO_2*. In these reactions, a purely asymmetric vibrational level v relaxes into a lower asymmetric level v – 1 with a symmetric sublevel a,b,c. It is assumed that symmetric sublevels relax rapidly via VT relaxation, thus becoming in thermal equilibrium with the asymmetric level. This mechanism is not a direct process and consists of multiple VT relaxation reactions, in which the first process is considered to be the rate limiting step [48]:

$$\left.\begin{matrix} CO_2(0\ 0\ v) + M \rightarrow CO_2(0\ 1\ v-1) + M \\ \rightarrow CO_2(0\ 2\ v-1) + M \\ \rightarrow CO_2(0\ 3\ v-1) + M \end{matrix}\right\} \xrightarrow{VT\ Relaxation} CO_2(0\ 0\ v-1) + M \quad \left.\begin{matrix} (V2a, Ref.[20]) \\ (V2b, Ref.[20]) \\ (V2c, Ref.[20]) \end{matrix}\right] \tag{70}$$

The rate constants are scaled by using expressions derived from the SSH theory [49, 50]. The scaling of the reaction rates is carried out by fitting the change of energy in the reaction to a diatomic anharmonic oscillator model. The rate constants of reactions involving higher vibrational levels v > 1 are estimated from the rate constant of the reaction corresponding to the lowest levels (from v = 1 to v = 0). The calculation procedure for scaling the reactions is adapted from [20].

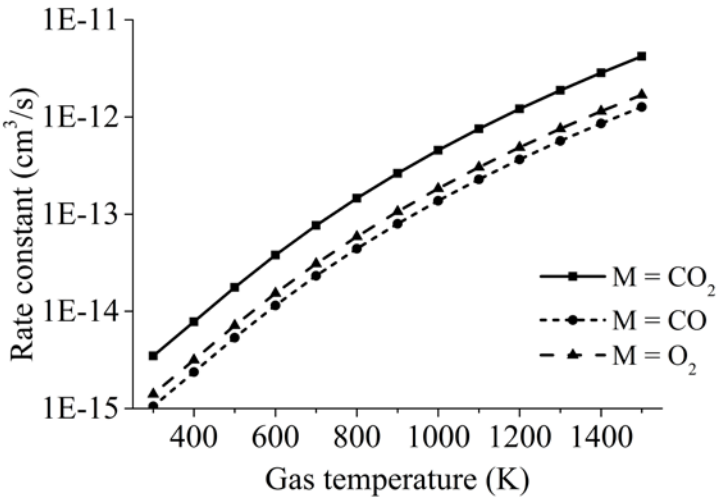

Fig. 7. Rate constant of reaction RV2 as function of gas temperature for M = CO_2, CO and O_2.

The reactions V2a,b,c [21] of all asymmetric vibrational levels within CO_2 are multiplied by the corresponding Treanor population and added to obtain three reactions per collision partner M:

$$\sum_{i=1}^{21}(n_i CO_2 v_i + n_i M) \rightarrow \sum_{i=2}^{21}(n_i CO_2 v_{i-1} + n_i M) + n_1 CO_2 v_{a,b,c} + n_1 M \tag{81}$$

by introducing the fictitious species CO_2* they can be simplified to

$$CO_2{}^* + M \rightarrow (1 - n_1) CO_2{}^* + n_1 CO_2 v_{a,b,c} + M \tag{92}$$

For a specific collision partner M it is possible to express these reactions in a more general "lumped" expression, which is more convenient for implementation into the model:

$$\begin{aligned} &CO_2{}^* + M \rightarrow v_{l2} CO_2{}^* + v_{s2}(CO_2 v_a + CO_2 v_b + CO_2 v_c) + M \\ &v_{l2}(T_g) = 1 - n_1(T_g), \quad v_{s2}(T_g) = \frac{1}{3} n_1(T_g) \end{aligned} \tag{103}$$

where v_{l2} and v_{s2} are the stoichiometric coefficients of the lumped excited state and the symmetric levels a,b,c respectively. The coefficients are function of the population density of the first asymmetric vibrational level n_1, which is computed with the Treanor distribution at a specific gas temperature T_g. The total averaged rate constant of the reaction RV2 (see Table 4) for a specific collision partner M is estimated by adding the averaged rate constants of the three individual reactions:

$$k_M(T_g) = k_{M,a}(T_g) + k_{M,b}(T_g) + k_{M,c}(T_g) \tag{114}$$

The averaged rate constant of each reaction is computed as in (9), considering that the individual rate constants k_v are scaled to the asymmetric vibrational level v, and depend on the symmetric sublevel

and the collision partner M. For each collision partner M, the temperature range of interest (300-1500 K) is evaluated as shown in Fig. 7. For each of the reactions with different collision partners, the rate constant is fitted to a modified Arrhenius equation with the aim of using a more practical expression in the model.

Rate constant for reaction RV3

The calculation process is similar to the one presented above for RV2. In this case, the energy is transferred between different vibrational modes, i.e. the asymmetric and the first two symmetric modes (a, b). The reaction scheme is represented as

$$\left.\begin{matrix} CO_2(0\ 0\ v) + CO_2 \rightarrow CO_2(0\ 2\ v-1) + CO_2(0\ 1\ 0) \\ \rightarrow CO_2(0\ 1\ v-1) + CO_2(0\ 2\ 0) \end{matrix}\right\} \left.\begin{matrix} (V5\ x = a, Ref.[20]) \\ (V5\ x = b, Ref.[20]) \end{matrix}\right] \quad (125)$$

Assuming a rapid VT relaxation of the symmetric sublevels and adding the reactions of all asymmetric levels within CO_2*, the following expression is obtained for V5 x = a:

$$\sum_{i=1}^{21}(n_i CO_2 v_i + n_i CO_2) \rightarrow \sum_{i=2}^{21}(n_i CO_2 v_{i-1} + n_i CO_2 v_a) + n_1 CO_2 v_b + n_1 CO_2 v_a \quad (16)$$

The reaction RV3 included in the model is a result of combining the previous reaction with the analogous reaction V5 for the symmetric level b. Once the two combined reactions are put together, RV3 can be written as:

$$\begin{aligned} &CO_2{}^* + CO_2 \rightarrow v_{l3} CO_2{}^* + v_{s3}(CO_2 v_a + CO_2 v_b) \\ &v_{l3}(T_g) = 1 - n_1(T_g), \quad v_{s3}(T_g) = \frac{1}{2}(n_1(T_g) + 1) \end{aligned} \quad (17)$$

The stoichiometric coefficients v_{l3} and v_{s3} are computed as done in the previous section for RV2. The total averaged rate constant of reaction RV3 is estimated by adding the individual averaged rate constants of both reactions:

$$k(T_g) = k_a(T_g) + k_b(T_g) \quad (18)$$

The averaged rate constant of each reaction is computed as in (9), considering that the individual rate constants k_v are scaled to the asymmetric vibrational level v and depend on the symmetric sublevel.

The overall "lumped" rate constant calculated at various temperatures is fitted to a modified Arrhenius equation to obtain a temperature-dependent expression (see Table 4).

The results of the rate constant obtained at various temperatures are displayed in Fig. 8.

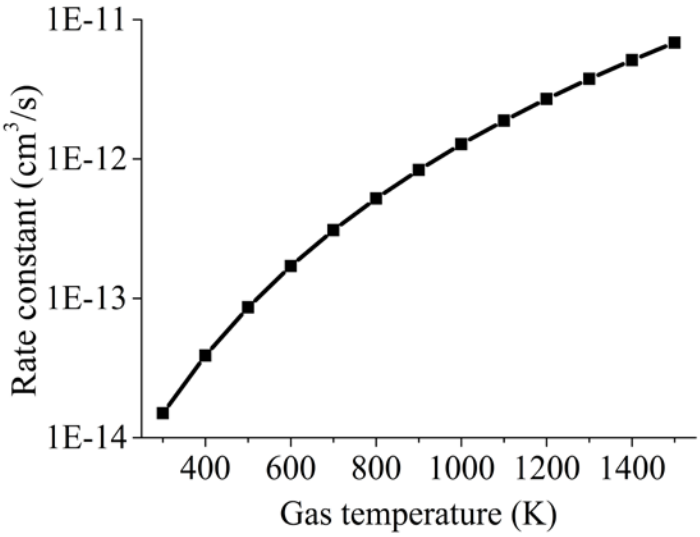

Fig. 8. Rate constant of reaction RV3 as function of gas temperature.

Surface reactions

These type of reactions take place on the surface of the reactor when chemical species collide with the surface. The rate coefficients for a single species can be determined by the following expression [51]:

$$k_s = \left(\frac{1}{1-\gamma/2}\right)\frac{\gamma}{(\Gamma_{tot})^s}\left(\frac{1}{4}\right)\left(\frac{8k_B T_g}{\pi m}\right)^{\frac{1}{2}} \tag{19}$$

where γ is the sticking coefficient of the reaction, i.e. the probability that the collision results in a reaction. Γ_{tot} is the total surface site density [1/m^2] and the exponent s is the sum of the stoichiometric coefficients of the surface reactants. The square root term is the mean thermal speed of the colliding species, computed from the Boltzmann constant K_B, the bulk gas temperature Tg and the mass of the species m. It is noted that the first term within the brackets is the Motz-Wise correction, which is only included when the sticking coefficient is large, i.e. close to 1 [51].

Various surface reactions can occur in the reactor, such as recombination or vibrational de-excitation reactions. The characteristic diffusion time is orders of magnitude smaller than the residence time of the reactor [21], thus recombination reactions on the wall can be neglected. In the latter, the collision frequency is high enough to ensure a dominant vibrational de-excitation through VT relaxation processes. For the abovementioned reasons, neither recombination nor vibrational de-excitation reactions are included in the model. The included surface reactions are related to recombination or neutralization processes through which ions are grounded (green arrows in Fig. 1 and Table 5) and restore the neutral charge. Due the low temperatures of heavy species, a unity sticking coefficient is assumed for these low energy collisions of ions with the walls [52, 53]. Moreover, ions are consumed in

these reactions and thus are needed to avoid their accumulation inside the reactor. The expression presented to calculate the rate coefficients can be simplified to the one shown below as no surface species are involved in the reactions:

$$k_s = \left(\frac{1}{1-\gamma/2}\right)\left(\frac{k_B T_g}{2\pi m}\right)^{\frac{1}{2}} \tag{20}$$

Results and discussion

In this section, a comparison of the results obtained from the proposed reduced model and the detailed STS kinetic model is performed. A qualitative study of the key model parameters is also carried out to identify which parameter displays the highest influence on the reduced model predictions. A simple reactor model was built in the COMSOL Multiphysics-plasma module [54] for this purpose. Spatially uniform quasi-neutral plasma is assumed throughout the reactor volume.

In the previous section, a description of the calculation process to estimate the rate constants for highly relevant chemical reactions in the dissociation kinetics of CO_2 is provided. In this regard, the computed rate constants for reactions involving the lumped excited species CO_2* are shown in Fig. 9. Two different zones are distinguished in this Figure. At low temperatures, below 700-800 K, the rate constants for the reactions with neutrals are relatively higher than the vibrational energy transfer reactions, thus leading to high dissociation rates of the CO_2 molecule. At high temperatures though, above 800 K, the vibrational reactions become dominant, resulting in a drop of the dissociation rate at the expense of increasing the bulk gas temperature.

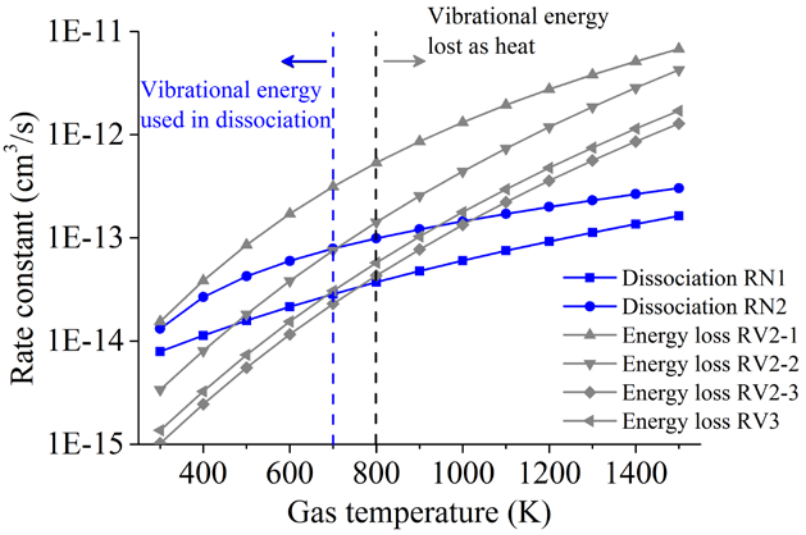

Fig. 9. Rate constants of the main reactions leading to dissociation of the CO_2 molecule (blue lines, RN1 and RN2) and the reactions causing energy loss (grey lines, RV2-1, RV2-2, RV2-3 and RV3).

Validation of the model

The simulations to investigate the validity of the reduced kinetic model are carried out at the same conditions as reported in [21]. The discharge takes place at a pressure of 100 torr, reduced electric field of 50 Td, electron density 10^{13} 1/cm^3, specific energy input 0.6 eV/molecule, frequency of the electromagnetic field 2.45 GHz and a residence time of 1.4 x 10^{-5} s. Elastic scattering and ionization reactions are not considered, and CO_2^+ is the only ion included for the quasi-neutrality of the plasma. The initial gas composition is a CO_2 mole fraction of 1; the initial bulk gas temperature is 300 K and the initial electron temperature is 0.39 eV or 4500 K.

In this work, the plasma medium is specified by the electron density and the mean electron energy. In the case of multidimensional simulations, where the spatial distribution and time evolution of the species concentration are to be studied, these parameters should be determined by solving the conservation laws and Boltzmann equation for the electrons. The energy equation is not included in the model. The electron and gas temperatures profiles in the reactor volume are specified as functions fitted to the results given in [21]. Viscosity effects are neglected and the pressure is considered uniform and constant inside the reactor.

Mass conservation equations are solved for the species to validate the reaction kinetics. Diffusion is neglected given its relatively short characteristic time. Thus, for this specific validation model the surface reactions are not included and the charged species densities are constant. This is done for consistency with [21], even though the results are not affected by the kinetics of charged species. Convection is not considered and time dependent simulations are performed based on the residence time value.

The model is divided into two parts describing two spatial zones; these are the plasma zone, where the plasma is active, and the afterglow zone, where the plasma vanishes. In the former, a constant electron density and an increasing electron temperature profile describe the chemically reactive (plasma) zone. In the latter, the electron density is set to zero, whereas a decreasing electron temperature profile is specified to describe the zone where reactive species relax back to equilibrium and radicals recombine. It is known that the electron density is not constant in either zone, but setting a constant electron density seems to be a good approximation to study the influence of chemical reactions in the overall reactive scheme. The total simulation time is fixed to 0.1 s, which is long enough for the relaxation process (VT and VV') to take place. In conclusion, the inputs required for the model are the electron density, electron temperature, bulk gas temperature and pressure. The comparison of the benchmark STS kinetic model versus the proposed reduced kinetic model is displayed in Fig. 10 where the division of both zones can be observed. As expected, the dissociation of CO_2 occurs mainly in the plasma zone, whereas recombination processes take place in the afterglow.

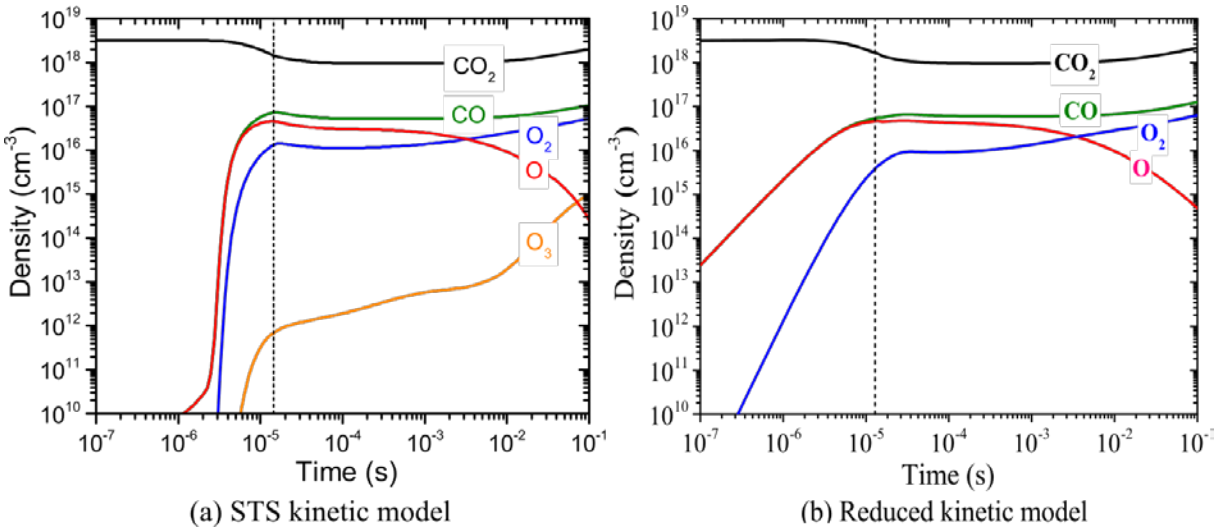

Fig. 10. (a) Population densities computed by the STS kinetic model, adapted from [21] **(b)** Population densities calculated by the reduced kinetic model of the most relevant neutral species

The major difference as for the computed species concentrations is found in the plasma zone. In the afterglow, the species densities are in good agreement with the STS kinetic model. Notably, the predicted CO_2 density is virtually exact in both models, which in turn allows the calculation of the CO_2 dissociation rate. On the other hand, the concentration of CO and O_2 present an error lower than 10% and 20%, respectively. The steep slopes noticed in the time range 10^{-6} – 10^{-5} in Fig. 10a are the result of the STS kinetic model. The processes by which the energy is transferred from the electrons to the lower levels of the vibrational ladder and then progressively transferred by VV relaxation to higher levels have a time scale of ~10^{-6} s. Once the highest vibrational levels are excited, the dissociation of CO_2 starts taking place until the VT relaxation rates become comparable to the VV relaxation ones at about 10^{-5} s and therefore the dissociation rate declines. In the abovementioned time range, the stored vibrational energy enhances the dissociation processes by lowering the activation energy of the reactions. The rate constants for the dissociation processes are rather high, which explains the sharp increase in the densities of CO and O. The increase in the O_2 concentration is mainly due to the O recombination reaction (RN5, Table 3). Concerning the reduced kinetic model, it is assumed that at low bulk gas temperatures, the lumped excited state CO_2* has a large population of the high vibrational levels, thus initiating the production of CO and O as soon as the species CO_2* is formed by means of electron collisions. This explains the slower dissociation process taking place in the reduced kinetic model in the range 10^{-7} to 10^{-5} s.

It is noticed that the predictions given by the model can be improved by adjusting the assumed value of the T_v/T_g ratio (Section 2.2, simplification approach) at low temperature. The value can be experimentally determined by measuring the vibrational and gas temperatures of the discharge, for instance, by optical emission spectroscopy [41]. This fact offers an evident benefit since the STS kinetic model does not enable such tuning due to the large number of reactions. At the very early stage in the

plasma zone (10^{-7}-10^{-6} s), the results of the reduced kinetic model do not match the ones from the STS model. Conversely, the densities calculated at the end of the plasma zone and the afterglow do match the predictions of the STS model. To validate other process conditions, the electron dynamics and the energy equation should be included in the model.

Effect of model parameters

The results presented in Fig. 10b are calculated using constant values of the following model parameters; scaling factor $\phi = 1.12$, stoichiometric coefficients $v_{l2} = 0.262$, $v_{s2} = 0.246$, $v_{l3} = 0.262$ and $v_{s3} = 0.869$ for a mean bulk gas temperature of 500 K in the discharge (plasma zone and afterglow). In Section 2, it was shown that these factors are function of the bulk gas temperature. As stated in [21], the gas temperature increases from 300 to 560 K over the residence time in the plasma zone; therefore an alternative mean bulk gas temperature of 300 K is considered to study the effect of these parameters on the model predictions. It was proven that the error induced by keeping the parameters constant is relatively small since the species concentrations follow nearly the same trends. In this regard, the effect of the T_v/T_g ratio at the initial gas temperature (300 K) as well as the assumed gas temperature at which thermal equilibrium is reached are evaluated and displayed in Fig. 11.

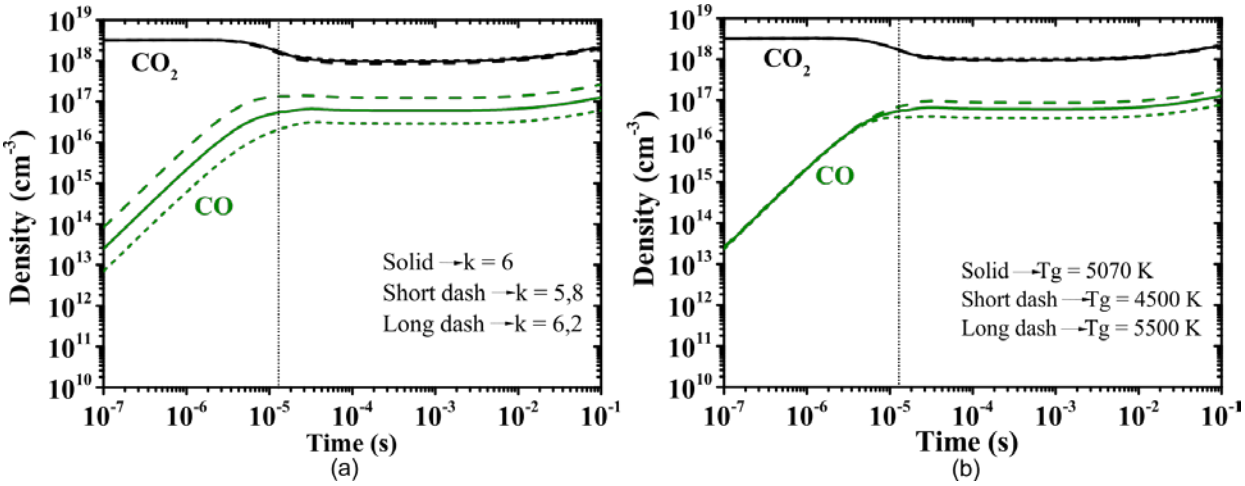

Fig. 11. (a) Population densities of CO_2 and CO for different T_v/T_g ratios (T_v/T_g = k) at constant gas temperature of 300 K and **(b)** population densities for constant T_v/T_g ratio (T_v/T_g = 6) considering different gas temperatures at which the plasma becomes thermal.

As expected, when the value of T_v/T_g is higher (T_v/T_g = 6,2 – long dash line) the dissociation rate increases and vice versa (T_v/T_g = 5.8 – short dash line). As previously stated, the value of T_v/T_g at low temperatures can be seen as the dissociation potential; the higher the T_v/T_g value the higher the vibrational energy stored in the molecules, thus conducting the process toward higher dissociation rates. The gas temperature at which the plasma becomes thermal seems to be much less influencing than the T_v/T_g ratio at low temperature. Lastly, it is shown that the value of T_v/T_g at low temperature

has a higher influence on the predictions of the CO_2 dissociation rate, whereas the gas temperature at which quasi-equilibrium plasma conditions are reached does not have a major effect on the overall process. In this regard, experimental validation of the concept proposed in this work, where the T_v/T_g values are taken from [21], needs to be carried through measurements of the vibrational and gas temperatures in a pure CO_2 microwave discharge via optical emission spectroscopy. However, the experimental determination of these two temperatures is complex and only approximate values can be obtained using current plasma diagnostic techniques. Lastly, the actual implementation of the proposed kinetic model has not yet been done in multidimensional simulations. The computation of local rate constants considering spatial variations of the T_v/T_g ratio can be highly complex. Hence, a better approach is to use a characteristic T_v/T_g value to describe the reactor performance and keep the computational load at its minimum.

Conclusions

We have introduced a new methodology to simplify detailed plasma vibrational kinetics and applied it to the dissociation of CO_2 in non-equilibrium microwave plasma discharges. In this type of discharges, the dissociation kinetics of the CO_2 molecule are driven by the excitation of the highest vibrational levels of the asymmetric streching mode. The novelty of the proposed model lies in four key elements; 1) the 21 vibrational levels considered for the asymmetric stretching mode are lumped within a single group, or fictitious species, CO_2*, 2) this group follows the so-called non-equilibrium Treanor distribution, 3) an algebraic approximation is used to compute the vibrational temperature from the translational temperature based on the Landau-Teller formula and 4) weighted algebraic expressions are applied, instead of complex differential equations, to calculate the rates of the most influencing reactions. The reduced kinetic model comprises 44 reactions among 13 species, as opposed to our benchmark detailed kinetic model, in which +100 species and +10000 reactions are considered, thus reducing substantially the calculation time to less than a minute. For the validation of the reduced kinetic model, a reactor model was built in COMSOL Multiphysics. The predictions of the reduced kinetic model showed that the neutrals densities are in good agreement with those predicted by the STS kinetic model, notably at the end of the plasma zone and the afterglow, which represent the reactor outlet.

The calculation process for the rate constants of the most influencing chemical reactions in the dissociation kinetics was described. Moreover, it was shown that the bulk gas temperature highly affects the dissociation rate as expected. Remarkably, at temperatures below 700 K, the dissociation rates are faster than the VT relaxation processes, thus resulting in higher conversion. Furthermore, a qualitative analysis of the key model parameters was carried out. The value of the T_v/T_g ratio at low

temperature had a considerable effect on the calculation process. This ratio can be used as a fitting parameter to link the presented plasma kinetic model to experimentally measured vibrational and gas temperatures via optical emission spectroscopy. At this stage of development, where current models are in qualitative agreement with experimental data, the introduction of an experimentally obtained parameter describing the non-thermal degree of the discharge can facilitate the transition from STS to more practical models suitable for engineering purposes. Furthermore, this parameter may be used to fit experimental data to the model, improving the overall accuracy of the predictions.

To further assess the influence of plasma/process parameters, the electron dynamics and energy equations should be included in the model. This will be the next step towards development of a self-consistent multidimensional model for non-thermal plasma reactors. As a final note, we believe that the presented approach can also be applied to other plasma chemistries, in which the vibrational kinetics are dominant in the dissociation process.

Acknowledgements

This research was supported by Alternative Energy Forms for Green Chemistry (ALTEREGO), an European cooperation project funded within the 7th Framework Programme with grant agreement No. 309874.

References

1 J. F. Griffiths, *Prog Energ Combust*, 1995, **21**, 25-107.

2 J. Amouroux, P. Siffert, J. P. Massue, S. Cavadias, B. Trujillo, K. Hashimoto, P. Rutberg, S. Dresvin and X. H. Wang, *Prog Nat Sci-Mater*, 2014, **24**, 295-304.

3 S. Sabihuddin, A. E. Kiprakis and M. Mueller, *Energies*, 2015, **8**, 172-216.

4 S. Hameer and J. L. van Niekerk, *Int J Energ Res*, 2015, **39**, 1179-1195.

5 T. M. I. Mahlia, T. J. Saktisandan, A. Jannifar, M. H. Hasan and H. S. C. Matseelar, *Renew Sust Energ Rev*, 2014, **33**, 532-545.

6 J. Amouroux and P. Siffert, *Spie Eco-Photonics 2011*, 2011, **8065**, 80650E.

7 Q. Wang, B. Spasova, V. Hessel and G. Kolb, *Chem Eng J*, 2015, **262**, 766-774.

8 J. R. Roth, *Indutrial plasma engineering* IOP Publishing Ltd: British Library, 1995.

9 R. Aerts, W. Somers and A. Bogaerts, *Chemsuschem*, 2015, **8**, 702-716.

10 H. H. Kim and A. Ogata, *Eur Phys J-Appl Phys*, 2011, **55**, 13806.

11 V. D. Rusanov, A. A. Fridman and G. V. Sholin, *Usp Fiz Nauk+*, 1981, **134**, 185-235.

12 A. Fridman, *Plasma Chemistry*, Cambridge: Cambridge University Press, 2008.

13 Y. G. Ju and W. T. Sun, *Prog Energ Combust*, 2015, **48**, 21-83.

14 Y. Yang, W. Hua and S. Y. Guo, *Phys Plasmas*, 2014, **21**, 040702.

15 M. Baeva, A. Bosel, J. Ehlbeck and D. Loffhagen, *Phys Rev E*, 2012, **85**, 056404.

16 M. Jimenez-Diaz, E. A. D. Carbone, J. van Dijk and J. J. A. M. van der Mullen, *J Phys D Appl Phys*, 2012, **45**, 335204.

17 P. Gokulakrishnan, R. Joklik, D. Viehe, A. Trettel, E. Gonzalez-Juez and M. Klassen, *J Eng Gas Turb Power*, 2014, **136**, 011503.

18 A. Cenian, A. Chernukho, V. Borodin and G. Sliwinski, *Contrib Plasm Phys*, 1994, **34**, 25-37.

19 E. V. Kustova and E. Nagnibeda, *Chem Phys*, 2006, **321**, 293-310.

20 T. Kozak and A. Bogaerts, *Plasma Sources Sci T*, 2014, **23**, 045004.

21 T. Kozak and A. Bogaerts, *Plasma Sources Sci T*, 2015, **24**, 015024.

22 G. van Rooij, D. van den Bekerom, N. den Harder, T. Minea, G. Berden, W. Bongers, R. Engeln, M. Graswinckel, E. Zoethout and M. van de Sanden, *Faraday Discuss*, 2015, **183**, 233-248.

23 A. Stagni, C. Saggese, M. Bissoli, A. Cuoci, A. Frassoldati, T. Faravelli and E. Ranzi, *Iconbm: International Conference on Biomass, Pts 1 and 2*, 2014, **37**, 877-882.

24 T. E. Magin, M. Panesi, A. Bourdon, R. L. Jaffe and D. W. Schwenke, *Chem Phys*, 2012, **398**, 90-95.

25 A. Guy, A. Bourdon and M. Y. Perrin, *Chem Phys*, 2013, **420**, 15-24.

26 H. P. Le, A. R. Karagozian and J. L. Cambier, *Phys Plasmas*, 2013, **20**, 123304.

27 L. F. Spencer and A. D. Gallimore, *Plasma Sources Sci T*, 2013, **22**, 015019.

28 K. Peerenboom, A. Parente, T. Kozak, A. Bogaerts and G. Degrez, *Plasma Sources Sci T*, 2015, **24**, 025004.

29 Y. Itikawa, *J Phys Chem Ref Data*, 2002, **31**, 749-767.

30 K. Kameta, N. Kouchi and Y. Hatano, in *Interactions of Photons and Electrons with Molecules*, ed. Y. Itikawa, Springer Berlin Heidelberg, 2003, vol. 17C, ch. 1, pp. 4001-4061.

31 A. Zecca, G. P. Karwasz and R. S. Brusa, *Riv Nuovo Cimento*, 1996, **19**, 1-146.

32 Y. Itikawa, *J Phys Chem Ref Data*, 2009, **38**, 1-20.

33 R. R. Laher and F. R. Gilmore, *J Phys Chem Ref Data*, 1990, **19**, 277-305.

34 H. T. Zheng and Q. Liu, *Math Probl Eng*, 2014, **vol. 2014**, 938618.

35 A. H. Markosyan, A. Luque, F. J. Gordillo-Vazquez and U. Ebert, *Comput Phys Commun*, 2014, **185**, 2697-2702.

36 G. Colonna, I. Armenise, D. Bruno and M. Capitelli, *J Thermophys Heat Tr*, 2006, **20**, 477-486.

37 G. Colonna, L. D. Pietanza and M. Capitelli, *J Thermophys Heat Tr*, 2008, **22**, 399-406.

38 A. Berthelot and A. Bogaerts, *Plasma Sources Science and Technology*, 2016, **25**, 045022.

39 C. E. Treanor, J. W. Rich and R. G. Rehm, *J Chem Phys*, 1968, **48**, 1798-&.

40 H. S. Kwak, H. S. Uhm, Y. C. Hong and E. H. Choi, *Sci Rep-Uk*, 2015, **5**, 18436.

41 T. Silva, N. Britun, T. Godfroid and R. Snyders, *Plasma Sources Sci T*, 2014, **23**, 025009.

42 L. D. Pietanza, G. Colonna, G. D'Ammando, A. Laricchiuta and M. Capitelli, *Chem Phys*, 2016, **468**, 44-52.

43 K. Anzai, H. Kato, M. Hoshino, H. Tanaka, Y. Itikawa, L. Campbell, M. J. Brunger, S. J. Buckman, H. Cho, F. Blanco, G. Garcia, P. Limao-Vieira and O. Ingolfsson, *Eur Phys J D*, 2012, **66**, 36.

44 S.J. Buckman, M.T. Elford, Mitio Inokuti, Y. Itikawa, and Hiro Tawara, *Interactions of Photons and Electrons with Atoms*, Springer-Verlag, Berlin/Heidelberg, 2000.

45 Y. Itikawa, *Molecular processes in plasmas*, Springer Series on atomic, optical and plasma physics, Vol. 43 (Springer Berlin Heidelberg), 2007.

46 R. D. Levine and R. B. Bernstein, in *Dynamics of Molecular Collisions*, ed. W. Miller, Springer US, 1976, vol. 2, ch. 7, pp. 323-364.

47 J. A. Blauer and G. R. Nickerson, *Report Ultrasystems, Inc*, 1973.

48 T. Kozák, *Private communication*, 2015.

49 R. N. Schwartz, Z. I. Slawsky and K. F. Herzfeld, *J Chem Phys*, 1952, **20**, 1591-1599.

50 J. Keck and G. Carrier, *J Chem Phys*, 1965, **43**, 2284-2298.

51 R. J. Kee, *Chemically Reacting Flows*, John Wiley & Sons, Inc., Hoboken, NJ, USA, 2003.

52 K. Hassouni, F. Silva and A. Gicquel, *J Phys D Appl Phys*, 2010, **43**.

53 A. J. Ryan, *Emerging Themes in Polymer Science*, The Royal Society of Chemistry, 2001.

54 *Plasma Module User's Guide COMSOL Multiphysics 4.4*, 2013.